Rock Mech. Rock Engng. (1993) 26 (1), 29—62

Rock Mechanics and Rock Engineering

Experimental Measurement of Surface Temperatures During Flame-Jet Induced Thermal Spallation

By

M. A. Wilkinson and **J. W. Tester**

Massachusetts Institute of Technology, Cambridge, U. S. A.

Summary

Thermal spallation is a method whereby the surface of a rock is rapidly heated causing small (100—1000 μm) flakes or spalls, to form. When applied to drilling, a supersonic, high temperature (2600 K) gas jet is directed at the rock to provide the heat source and sweep away the spalls.

Previous studies of thermal spallation drilling indicate that penetration rates of up to 30 m/hr (100 ft/hr), approximately ten times greater than commonly obtained using conventional rotary mechanical methods, can be achieved in competent, non-fractured hard rock such as granite. A total direct operating cost for drilling in granite using a flame-jet spallation drill was estimated by Browning (1981) to be approximately \$9/m in 1991\$ (about \$3/ft) compared to "trouble-free" well drilling costs for conventional rotary methods in similar rock to depths of 3 to 7 km (10000 to 21000 ft) of \$300 to \$900/m (\$100 to \$300/ft) (Tester and Herzog, 1990, 1992). The Browning estimates for spallation drilling are obviously optimistic in that they don't include capital costs for the rig and associated hardware. However, the substantially higher penetration rates, significantly reduced wear of downhole components, and the high efficiency of rock communition in comparison to rotary methods suggest that substantial cost reductions could be possible in deep drilling applications. For example, in the construction of hot dry rock geothermal power plants where rotary mechanical methods are used for well drilling to depths of (4 to 5 km), about half of the initial capital cost would be required for well drilling alone (Tester and Herzog, 1992).

The current study has focused on gaining a better understanding of both the rock failure mechanism that occurs during thermal spallation and the heat transfer from the gas jet to the rock surface. Rock mechanics modeling leads to an expression for the surface temperature during spallation as a function of rock physical properties and the incident heat flux. Surface temperature measurements and heat flux determination during laser and flame-jet induced thermal spallation are used to provide appropriate values of the "Weibull parameters" that statistically describe the size-strength relationship in granite. Use of these parameters allows one to accurately estimate surface temperatures required by the numerical simulation model to calculate heat and mass transport rates occurring in the flow field above the spalling rock surface.

Based on the results of this experimental study, we concluded that mechanically-determined Weibull parameters are not directly applicable to describe spallation failure phenomena caused by thermal stress. Under the extreme rapid heating conditions of flame-jet drilling, local overheating and possibly stress relief lead to higher temperatures than predicted using room temperature Weibull parameters. Nonetheless, the Weibull-based statistical model of failure can be utilized by empirically fitting the m and σ_0 Weibull parameters to match experimental measurements of spalling surface temperature as a function of applied heat flux. Correlations for steady state and onset spallation conditions were established with consistent results obtained for both laser and propane-oxygen flame jet heating.

1. Introduction

Thermal spallation can be broadly defined as fragmentation of the surface of a brittle solid into small disk-like flakes, called spalls, by rapidly heating a relatively small fraction of the solid (e. g. less than 10% of the exposed area). Thermal stresses arising from the tendency of the heated portion of the material to expand as temperature is increased cause failure to occur. When thermal spallation is used for drilling, a "flame-jet" like the one shown in Fig. 1 is commonly used to impart the high heat fluxes (typically greater than 1.0 MW/m^2) required and to sweep away the spalls (Browning, 1981 and Williams et al., 1988).

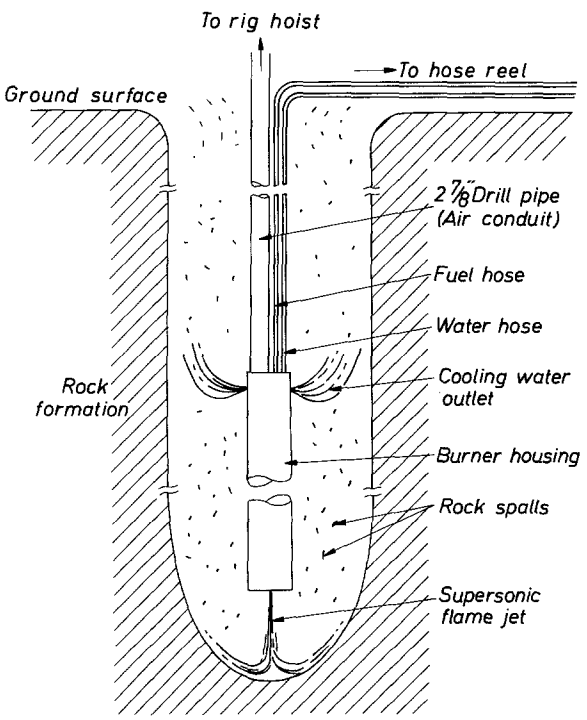

Fig. 1. Schematic of thermal spallation drilling (adapted from Williams et al., 1988)

Recent interest in the use of naturally occurring underground regions of hot dry rock (HDR) for power generation has resulted in a need for inexpensive, reliable drilling methods in hard, usually granitic, crystalline basement rock that is typically encountered (Armstead and Tester, 1987). The second law of thermodynamics limits the amount of useful work (electric power) that can be produced in such a heat mining process. The amount of electric power produced per unit of heat removed from the earth increases as the geothermal fluid (water) temperature increases. Since the temperature of the geothermal fluid is governed by the temperature of the hot underground reservoir and the earth's temperature usually increases with depth, the thermodynamically-limited maximum power generating capability of a HDR energy extraction system can normally be increased only by drilling deeper.

The high sensitivity of total geothermal power plant cost to drilling costs, combined with the inherent difficulties encountered when using conventional methods for these applications provides a strong economic incentive to explore alternative drilling techniques. As HDR well costs decrease, a larger fraction of the earth's available resource becomes commercially viable (see Tester and Herzog, 1990, for a quantitative discussion of these issues). In addition, other fields of interest including tunneling for transportation, cavity formation for energy storage, mining, deep-well drilling for waste storage and treatment, and oil and gas drilling in the overthrust belt would benefit from a rapid, inexpensive method for penetrating through crystalline rock.

In general, spallation drilling works best in rocks with high quartz (SiO_2) content, such as granite, quartzite, and some sandstones. These rock types are apparently able to build up the required compressive stresses, under rapid heating conditions, before stress relieving mechanisms such as softening or melting occur. A further requirement for good spallation drilling characteristics is that the rock mass being drilled be relatively free of macroscopic defects such as major fractures that would enable stress relief to occur. These requirements are met by most crystalline basement rocks that are encountered during deep (>1 km) well drilling. However, more typically encountered rocks such as limestone and shale, which are found in oil and gas well drilling, either are reported to spall very poorly, or not at all. Research aimed at extending the use of thermal spallation to these "soft" rocks is currently being conducted jointly by Los Alamos National Laboratory and the New Mexico Institute of Mining and Technology (Potter, 1988 and Williams et al., 1991). By producing a periodically heated surface, limestone was spalled at rapid rates.

Earlier work at MIT by Rauenzahn (1986) and Rauenzahn and Tester (1985, 1989, 1991 a, b) established the basis for this study. We have focused on characterization of fundamental mechanisms of spall formation and ejection and on modeling fluid flow and heat transfer processes important to simulating drilling and quarrying conditions observed in practice (Browning et al., 1965 and 1981; and Williams et al., 1988). A key objective was the prediction of penetration rate and borehole geometry as a function

of primary operating variables such as flame temperature, jet velocity, stand off distance, and the thermophysical properties of the rock.

2. Equations Governing Steady-State Thermal Spallation Drilling

2.1 Energy Balance

Knowledge of the heat flux and surface temperature at any point on the spalling surface allows determination of the local drilling velocity through a heat balance on the control volume surrounding the rock-gas interface. The heat balance can be written:

$$Q = (\rho\, C_p)_r\, U_{dr}\,(T_s - T_{r0}) + \Delta\, H_{pt} \tag{1}$$

$(\rho\, C_p)_r$ = rock thermal density (J/m³ K),
Q = heat flux to the rock (W/m²),
U_{dr} = local drilling velocity (m/s),
$\Delta\, H_{pt}$ = energy losses due to miscellaneous phase transitions and crack formation (W/m²),
T_s = local surface temperature (K), and
T_{r0} = initial rock temperature (K).

The second term on the right-hand side of Eq. (1) is assumed to be negligible during thermal spallation drilling.

2.2 Steady-State Hole-Shape Condition

In a somewhat idealized case of steady-state drilling, the average hole shape in the actively spalling region must remain constant and satisfy the condition that the forward component of the local penetration rate is, on average, the same everywhere. This is illustrated in Fig. 2 and can be expressed mathematically as:

$$V_{dr} = \frac{U_{dr}}{\cos(\theta)}, \tag{2}$$

where V_{dr} = forward advance rate of drill head (m/s), and θ = angle of the tangent of the rock boundary to the horizontal plane. By simple geometric reasoning, the hole shape is described by a solid of revolution defined by the cosine law of Eq. (2). The shape closely approximates a paraboloid of revolution.

In the present and earlier studies (Rauenzahn and Tester, 1989, 1991 a, b), computer fluid dynamics simulations have been developed for predicting the heat fluxes along the rock surface during thermal spallation drilling. Comparison of heat flux and hole diameter predictions with experimental results is accomplished by forming non-dimensional Stanton

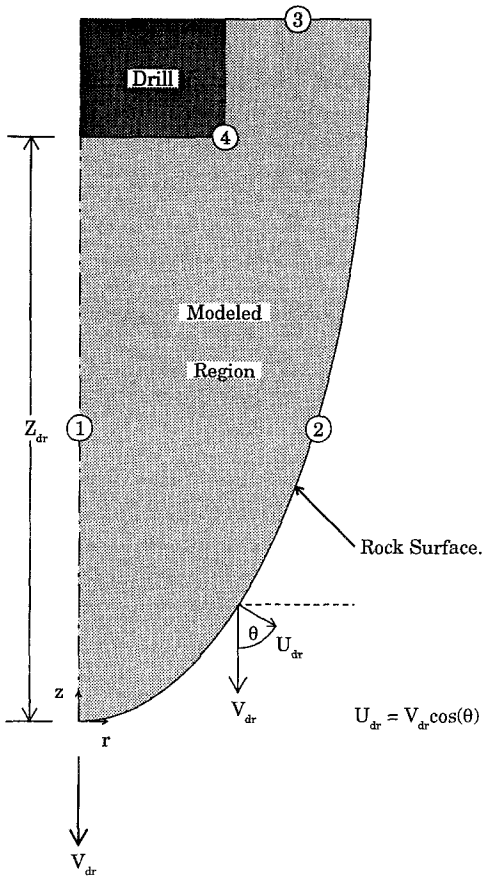

Fig. 2. Illustration of modeled region and self-consistency condition (Eq. (2))

numbers and hole radii (see Wilkinson and Tester, 1993). In this case, the Stanton number (St) is defined as the ratio of the rock surface heat flux (Q_r) to the total jet inlet heat flux (Q_{jet}), or:

$$St \equiv \frac{Q_r}{Q_{\text{jet}}} \tag{3}$$

and

$$Q_{\text{jet}} = (\rho\, C_p\, U)_{\text{jet}}\,(T_{\text{jet}} - T_s), \tag{4}$$

where T_{jet} is the temperature at the nozzle outlet. In order to determine the Stanton number from an experimentally measured penetration rate (V_{dr}), Q_r is calculated from Eq. (1) giving:

$$St_{\text{exp}} = \frac{(\rho\, C_p)_r\, V_{dr}\,(T_s - T_{r0})}{(\rho\, C_p\, U)_{\text{jet}}\,(T_{\text{jet}} - T_s)}. \tag{5}$$

Computer fluid dynamics simulation results predict directly the rock surface heat flux so that predicted Stanton numbers are given by

$$St_p = \frac{Q_p}{(\rho\, C_p\, U)_{\text{jet}}\,(T_{\text{jet}} - T_s)}, \tag{6}$$

where Q_p = predicted heat flux.

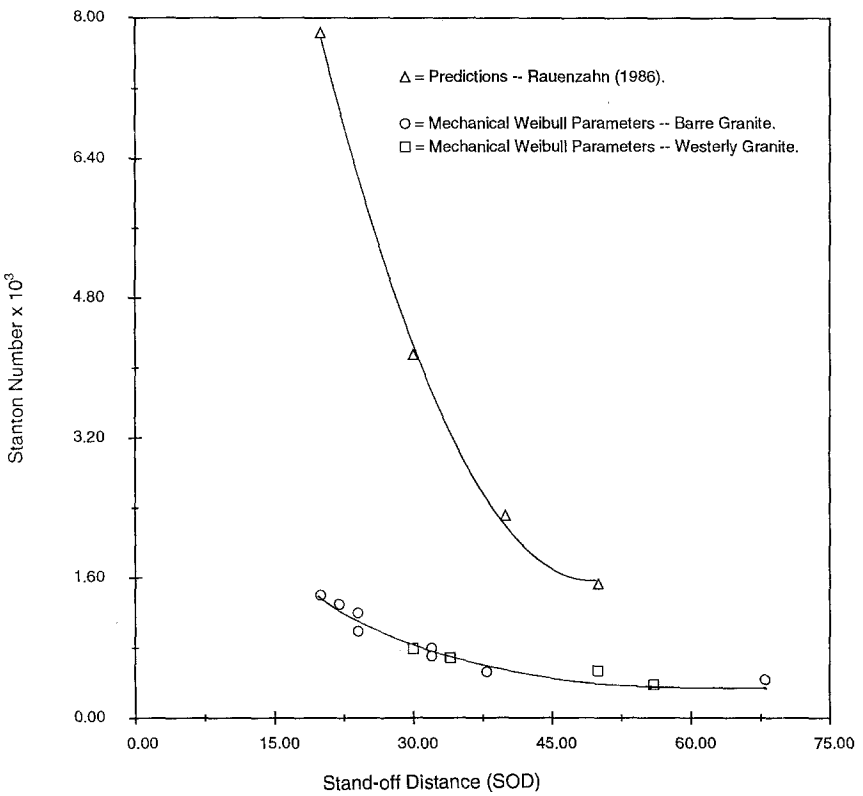

Fig. 3. Experimental and predicted Stanton numbers versus stand-off distance (Rauenzahn and Tester, 1991b)

Figure 3 shows earlier results for predicted and experimental Stanton numbers as a function of the non-dimensional drill head stand-off distance (*SOD*) defined as (see Rauenzahn and Tester, 1991a):

$$SOD \equiv \frac{Z_{dr}}{R_{\text{noz}}}, \tag{7}$$

where Z_{dr} = distance from bottom of drill to bottom of hole, and R_{noz} = nozzle inside radius. Predicted Stanton numbers (St_p) were from three to five times greater than the experimental ones (St_{exp}). Such a large discrepancy provided the major motivation for this investigation.

3. Objectives

The main goal of thermal spallation drilling research at MIT is to develop the ability to accurately predict thermal spallation drilling performance characteristics, for example forward drilling rate and hole radius. Forward drilling rate and hole radius are both governed by local drilling velocities on the rock surface, which can be calculated from predicted values of local heat fluxes (Q), or from experimental values of penetration rate, hole shape, and rock surface temperatures (T_s) through Eq. (1). Therefore, the specific objectives of the present study were:

1. to test a thermal spallation model (described below) that predicts rock surface temperature as a function of the applied heat flux (Dey and Krantz, 1985 and Rauenzahn and Tester, 1985, 1989), physical properties of the rock, and two empirical fitting parameters, and
2. to determine appropriate values of the fitting parameters for use in a computer fluid dynamic simulation of thermal spallation drilling.

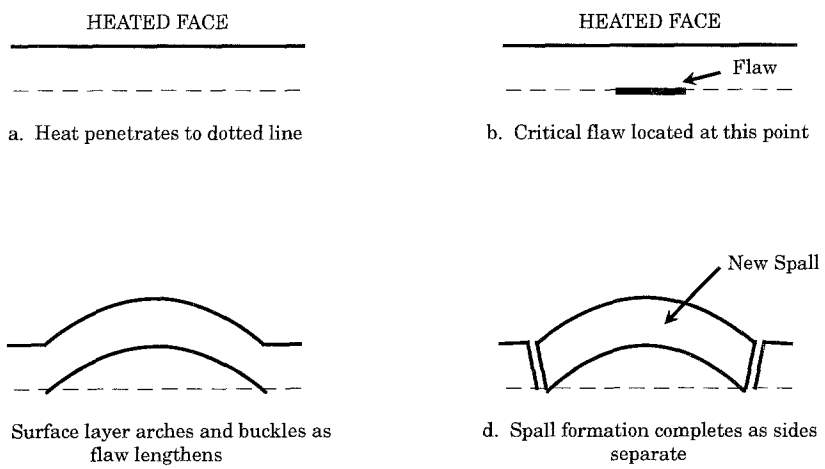

a. Heat penetrates to dotted line

b. Critical flaw located at this point

c. Surface layer arches and buckles as flaw lengthens

d. Spall formation completes as sides separate

Fig. 4. Simplified chain of events leading to spall formation on a surface of a semi-infinite solid (adapted from Preston, 1934)

4. Analysis of Rock Failure During Thermal Spallation Drilling

Preston (1934) was the first to propose the currently accepted mechanism for spall formation. Preston's mechanism, shown in Fig. 4 (Rauenzahn and Tester, 1989), is as follows:

1. a pre-existing flaw, near a surface, is acted upon by a compressive stress (thermally induced in the case of thermal spallation).
2. the flaw propagates in the direction of the applied stress, and parallel to the free surface.
3. the high aspect ratio (diameter to thickness) of the resulting plate and the high compressive stress cause buckling to occur, forming a "spall".

Although the mechanism described above is useful for providing a qualitative image of the processes occurring during thermal spallation, it does not describe the real situation where two or more flaws of various orientations and lengths may interact and when certain components of the rock do not undergo brittle failure at the conditions of interest.

With the above mentioned uncertainties in mind, Dey (1984) developed a mathematical description of the initiation of spallation based upon four underlying assumptions:

1. compressive failure occurs during spallation,
2. the stress level at failure is governed by the orientation, size, and number density of pre-existing flaws,
3. the Weibull statistical failure theory describes this stress level distribution, and
4. the temperature field can be approximated as being one-dimensional and treated as that at a subliming solid/gas interface.

Weibull theory considers that there is a failure probability associated with a given sample under stress such that the cumulative probability of failure $G(\sigma)$ is given by (Weibull, 1939):

$$G(\sigma) = 1.0 - \exp\left[\int_0^V (\sigma/\sigma_0)^m \, dV\right], \tag{8}$$

where σ = compressive stress (MPa)
σ_0 = compressive strength of rock per unit solid volume (MPa $-$ m$^{3/m}$),
V = sample volume under stress (m^3), and
m = homogeneity factor.

Integration of the right-hand side of Eq. (8) requires knowledge of the stress distribution within the sample volume. Assuming elastic behavior of the rock, a uniform surface temperature (T_s) and heat flux (Q), and that each spall is shaped like a cylinder with diameter to thickness ratio C_L leads to the following expression for the median surface spallation temperature (where $G(\sigma) = 0.5$) (Dey, 1984 and Rauenzahn and Tester, 1989):

$$T_S = T_r 0 + \left[\left(\frac{Q}{\rho C_p}\right)^3 \left(\frac{(1-\nu)\,\sigma_0}{\beta_r E}\right)^m \left(\frac{2\,(0.693)}{\pi C_L^2}\right) \left(\frac{m}{\alpha_r}\right)^3\right]^{1/(m+3)}. \tag{9}$$

E = Young's modulus (MPa),
ν = Poisson's ratio,
α_r = thermal diffusivity of the rock (m^2/s), and
β_r = thermal coefficient of expansion ($V^{-1}\,(\partial V/\partial T)_p$) ($K^{-1}$)

All physical properties and the Weibull strength parameters, m and σ_0, were considered to be temperature independent when deriving Eq. (9).

Therefore, the parameter values that are currently used for making calculations with Eq. (9) must be considered as temperature-averaged in some sense.

5. Experimental Procedures

5.1 Background

Use of the theory described in the previous section to estimate the rock surface temperature during thermal spallation drilling requires Weibull parameters: m and σ_0 values. Dey and Kranz (1985) performed mechanical tests at ambient temperature on Berkeley "blue" Granite. Rauenzahn and Tester (1989) studied thermal spallation on Westerly and Barre Granite using a 500 W CO_2 laser and a calibrated welding torch as heat sources. Both studies estimated values of $m \approx 20$ and $\sigma_0 \approx 70$ MPa $-$ m$^{3/20}$. An acetylene-oxygen flame was used as the heat source in the welding torch experiments; experimental details are provided by Rauenzahn and Tester (1989). Welding torch results are displayed in Fig. 5 and compared to those

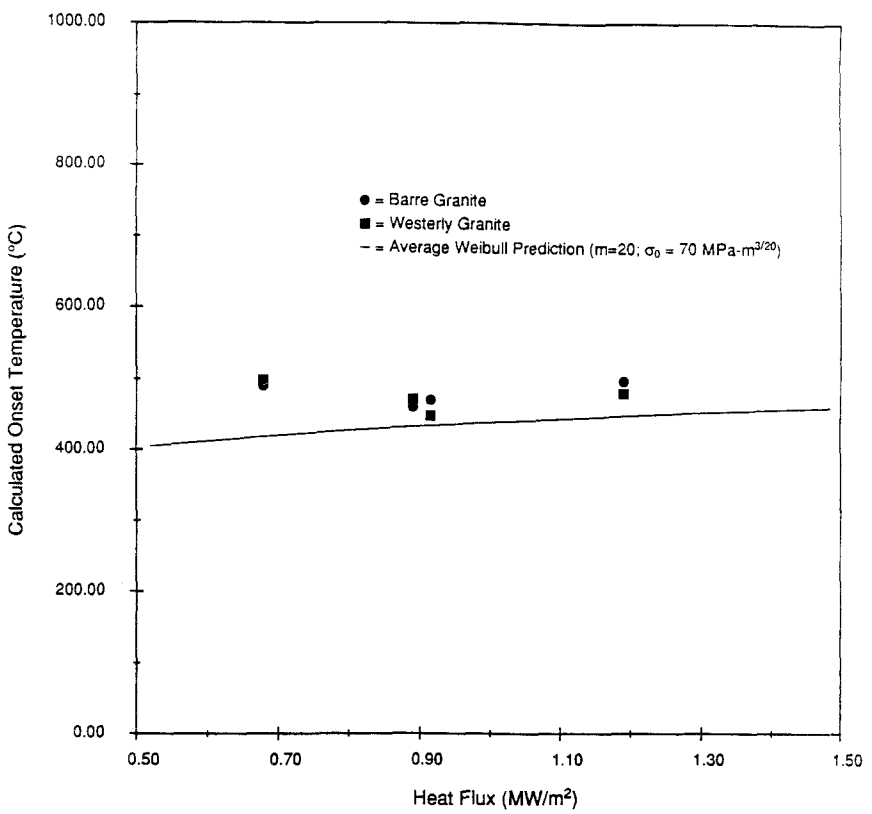

Fig. 5. Calculated spallation onset temperature versus calibrated heat flux during welding-torch heating (Rauenzahn and Tester, 1989)

obtained using Eq. (9) with the fitted Weibull parameters. Rauenzahn and Tester estimated spallation temperatures by recording heating tests on high speed videotape at 2000 frames per second and reviewing the tapes to determine the time required for the first spall to appear on the surface. The rock was assumed to behave as a one-dimensional, semi-infinite solid subjected to a constant heat flux (Q) as described by Carslaw and Jaeger (1959):

$$T_s = T_{ro} + 2\frac{Q}{k_r}\left(\frac{\alpha_r t}{\pi}\right)^{1/2} \tag{10}$$

where k_r = rock thermal conductivity (W/m K), α_r = rock thermal diffusivity (m^2/s), and t = time (s).

Therefore, knowing the heat flux and the time taken for the onset of spallation, the surface temperature (in K) was estimated from Eq. (10). However, using the first spall as the criterion for determining the "spallation temperature" complicates interpretation of temperatures so obtained. In the context of the theory described in the previous section, spallation occurs at a distribution of stress levels and the spallation temperature is defined as that occurring at the median cumulative probability of failure. The first spall to appear represents an initiation phenomenon characteristic of the "weakest" flaw at the low-end tail of the failure stress distribution where spalling temperatures are expected to be below the median spallation temperature. Ideally, random points on a surface heated with a spatially uniform heat flux should be chosen and the surface spallation temperatures averaged for determination of a more representative median spalling temperature.

Rauenzahn and Tester point out that difficulties also arise from the small beam diameters used during their laser heating tests. A typical beam heat flux profile obtained from the burn pattern produced in a plexiglass sample reveals an inner constant heat flux region surrounded by an outer linearly decreasing flux from r' to r'' (Rauenzahn, 1986). The two values of inner radius (r') obtained in this study were 0.5 and 2.0 mm while the outer radius (r'') varied from 5.0 to 8.0 mm. The one-dimensional heating assumption used in deriving Eq. (9) is violated by both of these beam radii because the depth of the heated region is on the order of 1 mm which is close to the beam diameter.

Furthermore, the small volumes that are heated may not include enough flaws and grains for the Weibull-based theory developed by Dey (1984) to adequately describe the statistics of the failure processes occurring.

Experiments performed in the present study were aimed at avoiding the difficulties described above. Laser and flame-jet induced thermal spallation have been performed in several well-characterized rock types while monitoring surface temperatures with a commercially available infrared (IR) scanner. A high powered (25 kW) CO_2 CW laser with an annular beam having a 4 to 1 outside-to-inside diameter ratio was used so that large over-

all diameters of 5 and 15.8 cm could be achieved while maintaining heat fluxes in the important range from about 0.1—3.0 MW/m^2. In addition, larger beam diameters provided more representative samples of rock surface, comparable to those encountered in the torch experiments. The heat source for flame-jet spallation tests was the propane-oxygen torch used by Rauenzahn during his small-scale field drilling experiments.

The specific experimental objectives were:

1. to extend the range of heat fluxes at which spallation temperatures in common granite rocks have been measured,
2. to take direct surface temperature measurements during thermal spallation,
3. to obtain accurate values for heat fluxes at these temperatures, and
4. to verify that the rock failure mechanism occurring during flame-jet and laser induced thermal spallation are similar.

5.2 Flame-Jet Spallation Experiments

Figure 6 is a schematic diagram of the experimental set-up that was used during flame-jet spallation tests. An infrared (IR) scanner was used for

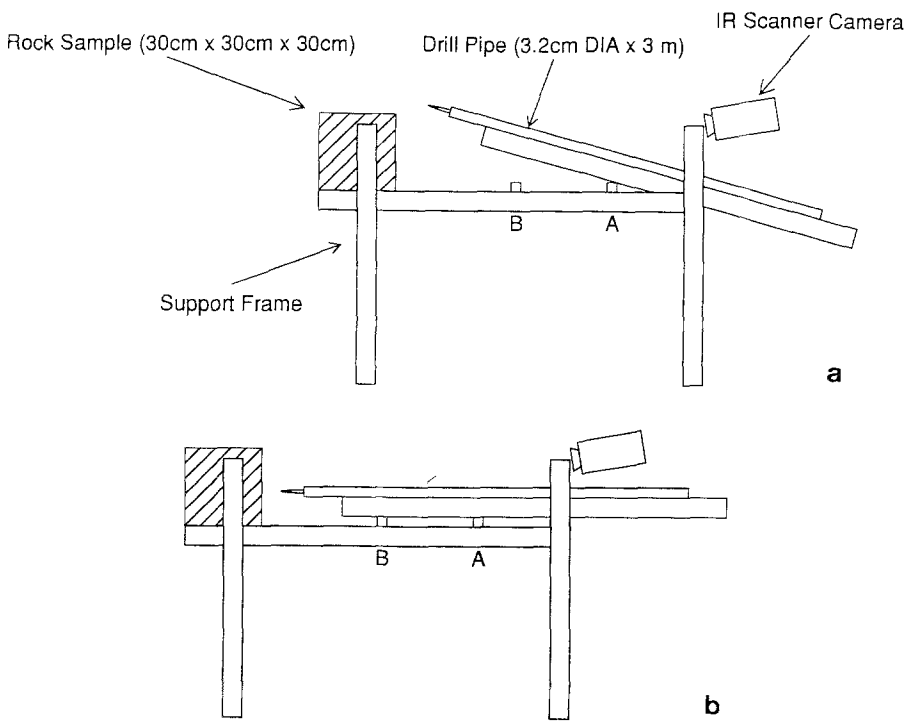

Fig. 6. Small-scale flame-jet spallation experimental set-up, **a** torch in raised position, **b** torch in lowered position

non-contact surface temperature measurement. A Unistrut beam supported the torch and acted as a hinge to the table at point "A" so that the torch could be quickly moved to and from the sample during operation. Guides at point "B" assured that the torch was correctly positioned when it was lowered, as shown in Fig. 6b. Parts of the support frame exposed to hot gases were wrapped in 2.54 cm (1 inch) thick refractory ceramic fiber in order to protect them from the intense heat. A one-inch thick refractory board protected the sample while the torch was being lowered into position.

The torch was ignited in the "upright" position, shown in Fig. 6a, by opening the propane flow control valve slightly and passing a flame underneath the nozzle outlet. Once lit, the oxygen flow rate was slowly increased until a characteristic "pop" was heard, indicating that the flame had flashed-back to the internal flame-holder, whereupon both flow control valves were completely opened.

After several minutes of operation the torch was stabilized and the infrared scanner was started. The torch was lowered into position by one operator, while another held the protective board in place. The protective board was pulled away in about 0.1 seconds and spalling occurred within 0.1 to 20 seconds depending on the stand-off distance of the burner head from the rock sample. Rock samples were either turned to expose a new face, or removed after each experiment.

Barre and Westerly granite were used in these tests. All Barre samples were 0.3 m × 0.3 m × 0.3 m (1 ft × 1 ft × 1 ft) and Westerly samples varied in cross section and thickness from about 0.3 m × 0.3 m × 0.1 m (1 ft × 1 ft × 0.3 ft) to 0.9 m × 0.3 m × 0.15 m (3 ft × 1 ft × 0.5 ft). Table 1 lists the petrographic mineral compositions of Barre and Westerly granite (Krech et al., 1974).

Table 1. Mineral compositions as weight percent of Barre and Westerly granite

Mineral	Barre granite	Westerly granite
Plagioclase	50.0	43.0
Quartz	22.0	24.6
Microcline	10.0	22.0
Biotite	8.0	6.9
Muscovite	6.0	2.0
Other	4.0	1.5

5.3 Laser-Heating Tests

The experimental laser set-up consisted of the laser, associated optics, an optical beam spinner, and a focusing head as illustrated in Fig. 7. The infrared scanner and a Kodak Ektapro 1000 high speed videotaping unit, capable of recording at 1000 frames/s, were used for data acquisition.

The laser and associated hardware were set-up by personnel at United Technologies Industrial Lasers in East Hartford, Connecticut. An optical

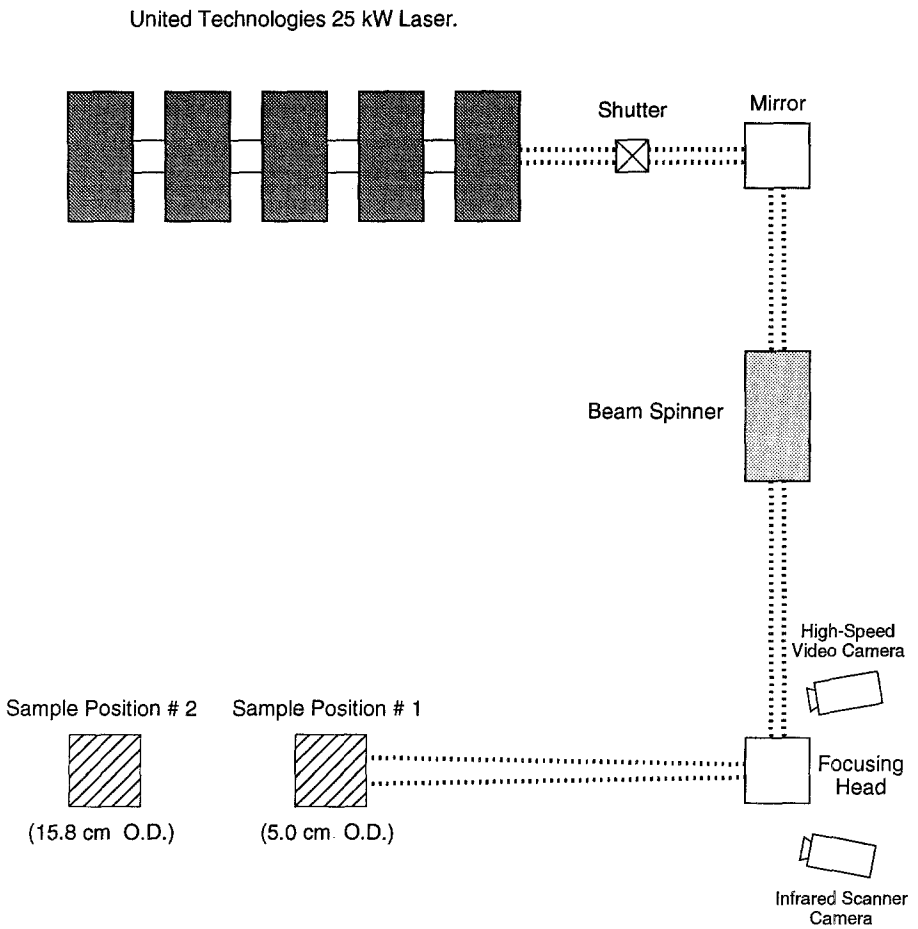

Fig. 7. Schematic of experimental set-up for laser-induced spallation (not to scale)

beam spinner was used to smooth azimuthal non-uniformities in the raw laser beam by rotating the beam at 4000—6000 rpm. The focusing head put a slight angle of divergence on the beam so that beam impingement diameters could be easily varied by changing the distance from the sample to the head. The pattern created by the laser beam was an annular ring with an outside-to-inside diameter ratio of approximately 4 to 1. The beam impingement time was controlled by user-defined settings in a numerical controller machine that sent electrical impulses to open or close the external shutter that was positioned in the path of the laser beam. High speed videotapes reveal that the shutter took approximately 50 ms to fully open.

The operating procedure was as follows:

1. Position and label rock sample
2. enter laser power level and time of irradiation into numerical controller

3. start infrared scanner and high speed videotaping unit, and
4. open shutter

All laser settings were recorded, and before and after photographs of samples were taken.

5.4 Surface Temperature Measurement Using IR Scanning

The radiation emitted from the surface of a body is a function of its temperature. When an infrared scanner device is used, this radiation is measured and the surface temperature determined without the normal requirement of physical contact between the temperature sensor and the object being measured. Several researchers have attempted to measure spallation temperatures by implanting thermocouples in the rock and monitoring the transient temperature rise up to the time when the thermocouple fails due to contact with the flame (Thurumalai, 1969). The major problems associated with this technique are: inaccuracies because thermocouple bead diameters are typically about the same size as the heated layer thickness (approximately 1 mm), local rock weakening resulting from drilling the holes that contain the thermocouples, and poor thermal contact between the thermocouples and the rock samples due to the different thermal expansion characteristics of the thermocouple bead and the rock. Furthermore, a large number of thermocouples must be used to obtain lateral surface temperature distributions.

The IR scanner provides direct surface temperature measurements at a sampling frequency of 20 Hz and a spatial resolution of 240 horizontal $\times$ 512 vertical zones. The temperature information is displayed as colors on a video screen and a color key allows conversion back into temperatures. In addition, a screen cursor displays a direct digital temperature value at a user-chosen point of interest. The principles of operation of the IR scanner used for the present study are described by Wilkinson (1989).

5.5 Independent Calibration of IR Scanner

The accuracy of the IR scanner for this application is dependent upon using the correct surface emissivity for the rock and minimizing atmospheric attenuation between the rock and the scanner lens. Furthermore, when the flame-jet is being used as a heat source, reflection of the radiation transmitted from the hot gases to the surface must be accounted for. Reflected radiation should be unimportant during laser heating because the laser emits monochromatic light at 10.6 μm which is well above the 5.6 μm upper detection limit for the IR scanner. In the present study, the accuracy of the IR scanner was checked by performing calibration experiments.

The first calibration experiment was aimed at verifying the ability of the IR scanner to accurately measure granite surface temperatures in the range expected during spallation. A 1.9 cm diameter $\times$ 4.5 cm long cylin-

der of granite with emissivity 0.90 was heated in a tube furnace (Fig. 8) and the rock surface temperature was measured using a type K thermocouple positioned at the center of the tube. The rock surface temperature was approximately equal to the air temperature in the tube after one hour of heating. Unfortunately, only two high temperature measurements were recorded because of time and budget limitations. Deviations between thermocouple readings and IR scanner readings are 1.2% and 0.42% at 563 °C versus 569.5 °C and 592 °C versus 594.5 °C respectively. These errors are of the same order of magnitude as the intrinsic uncertainty associated with the thermocouple measurements.

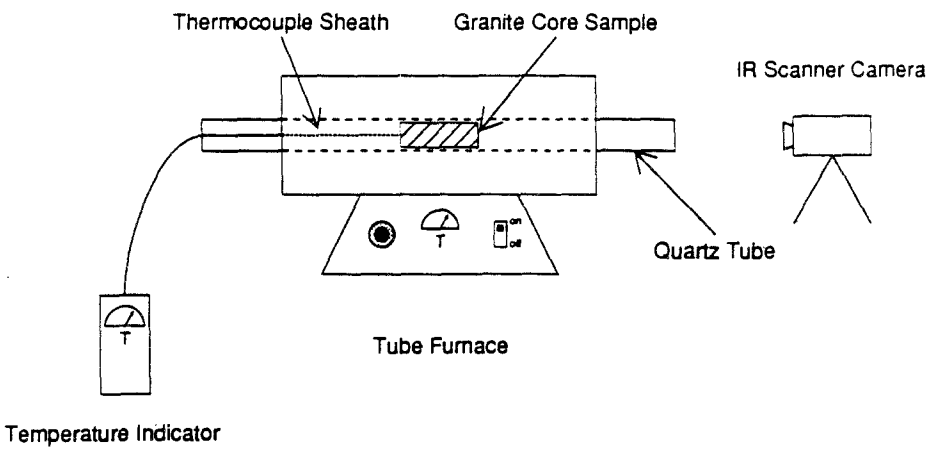

Fig. 8. IR scanner calibration set-up

In addition to these experiments, field calibrations were performed after some of the flame-jet and laser heating tests on Barre and Westerly granite, Sioux quartzite, and Webatuck dolomite by placing a thermocouple firmly against the rock surface when it had cooled to between 40—100 °C. Although these calibrations were less precise than the tube furnace tests, in all cases the thermocouple and IR scanner results were within 10% of each other and temperatures indicated by the thermocouple were always lower.

A final set of calibration tests were aimed at quantifying the effect of radiation from the high temperature gas stream that issued from the burner nozzle at about 2830 K and passed across the relatively cool rock surface from which temperature measurements were being taken. The high temperature gas stream was primarily CO_2 and H_2O. Monochromatic gas emissivities for CO_2 and H_2O vary widely over the electromagnetic wave-length spectrum and with the mean beam length of the gas making *a priori* determination of the cumulative interference over all wavelengths from 3.2 to 5.6 μm difficult. However, the black-body radiation flux at 2830 K is 3.6 MW/m^2 compared to about 50 kW/m^2 at typical rock surface temperatures. Thus, the potential for "flame" interference cannot be ignored.

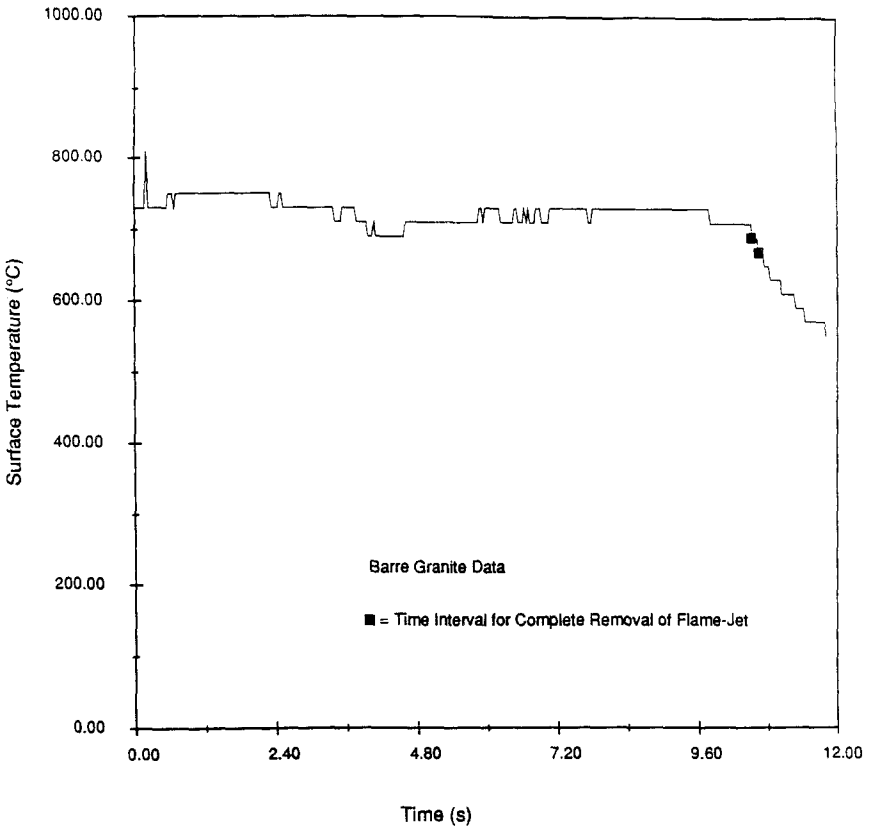

Fig. 9. Effect of flame radiation on IR scanner determined surface temperatures (Time interval contained between solid squares)

The influence of the propane/oxygen torch used in this study on the accuracy of surface temperatures measured during flame-jet tests has been estimated by allowing steady-state spallation to develop and then rapidly removing the torch from the rock sample while simultaneously monitoring the temperature-time history of the rock. The results of one such test are plotted in Fig. 9. Spallation temperatures measured by the IR scanner varied between about 710 °C and 730 °C while the torch was impinging upon it. When the torch was removed the indicated temperature dropped by 10—20 °C or about 2% within 50 ms and then continued to decrease at a similar but declining rate until observations were stopped approximately 1 s later. As described above, the IR scanner was calibrated at approximately 600 °C so that high accuracy is expected in the 710 to 730 °C range. Therefore, since some cooling occurred between measurements, the 2% temperature drop observed immediately after torch removal is a conservative upper limit estimate for the effect of flame interference on the indicated steady-state surface temperatures. Similar small initial temperature drops have been obtained for all flame-jet spallation experiments regard-

less of the torch stand-off distance or rock type. Therefore, the effects of flame interference on results reported in their study are assumed to be negligible.

6. Heat Flux Calculation Procedures

Validation of Eq. (9) and determination of the Weibull parameters requires that T_s be known as a function of the heat flux (Q). The most common methods of determining the heat flux to a surface are: measurement of the steady-state cooling requirement for a sensor of known surface area, and measurements of the temperature gradient across a substance with a known thermal conductivity and a one-dimensional temperature profile. Both of these methods are impractical for conditions on the rock surface during flame-jet or laser induced spallation because they require that sensors be mounted in the hostile environment existing at the rock surface during heating. Furthermore, the heat flux to the sensors is likely to be substantially different from that to the rough rock surface. Finally, before steady-state spalling conditions could be established in a given rock sample its surface would probably have receded past surface-mounted sensors.

With the above limitations in mind, several methods have been used to determine the heat fluxes in this study. In the first method the rock is again modeled as a one-dimensional, semi-infinite solid subjected to a constant heat flux at the free surface. The relationship between surface temperature and heating time is given by Eq. (10). Transient temperature rise data have been recorded for some of the flame-jet and all of the laser induced spallation experiments. Therefore, a least-squares line-fitting technique is used to match experimental curves of T_s versus $t^{1/2}$ to Eq. (10). The heat flux is related to the slope of this line as follows:

$$Q = \frac{A k_r}{2 (\alpha_r / \pi)^{1/2}}, \tag{11}$$

where A = slope of "best-fit" line. All temperature values used are taken from the digital cursor read-out on the IR scanner to avoid the subjectivity that would be inherently introduced otherwise when matching displayed colors to the color key. An example of the results of a calculation to determine the best-fit line through the T_s versus $t^{1/2}$ data and the heat flux for a laser heating test is illustrated in Fig. 10. The good fit of the data lends support to the one-dimensional temperature profile assumption made in deriving Eq. (10).

A second heat flux calculation method has been used for analyzing the flame-jet spallation data from measured drilling rates (V_{dr}) and steady-state stagnation-point surface temperatures ($T_{s,\,st}$). The drilling rate data obtained by Rauenzahn and Tester (1991b) were used to gen-

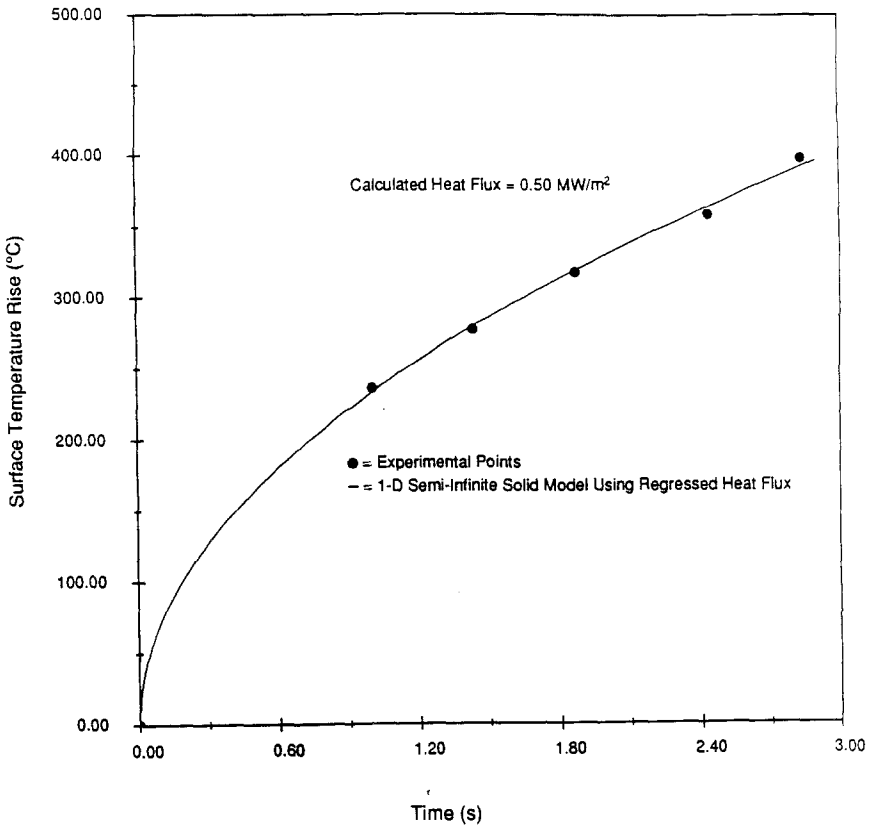

Fig. 10. Example of transient temperature rise curve for laser heating

erate a correlation of measured drilling rate versus standoff distance. The rock surface temperatures measured in the present study were then correlated to the estimated drilling rates based on measured standoff distances using the empirical Rauenzahn and Tester rate vs. standoff distance curve. The heat flux was calculated using Eq. (1) with ΔH_{pt} set to zero. Results are tabulated in Table 2 for Barre and Westerly granite. The stagnation-point heat flux obtained at a given stand-off distance during steady-state drilling experiments conducted by Rauenzahn (1986) is assumed to be equal to that at the stand-off distance on a flat granite surface. Furthermore, surface phase transformations and crack propagation energies are assumed negligible (ΔH_{pt} was set to zero in Eq. (1)).

Table 2. Results of small-scale quarry drilling tests from Rauenzahn (1986) and Rauenzahn and Tester (1991b)

Barre granite

Measured			Non-dimensionalized	
Drilling velocity V_{dr} (m/hr)	Stand-off distance Z_{dr} (cm)	Hole radius R_h (cm)	SOD Z_{dr}/R_{noz}	Hole radius R_h/R_{noz}
6.77	6.4	3.2—3.5	20	10—11
7.31	7.0	3.5	22	12
6.31	7.6	3.8	24	12
5.49	7.6	3.8—4.4	24	12—14
4.57	10.2	5.7—6.4	32	18—20
4.11	10.2	6.4—7.0	32	20—22
3.25	12.0	7.6	38	24
2.74	21.6	8.9	68	28

Westerly granite

Measured			Non-dimensionalized	
Drilling velocity V_{dr} (m/hr)	Stand-off distance Z_{dr} (cm)	Hole radius R_h (cm)	SOD Z_{dr}/R_{noz}	Hole radius R_h/R_{noz}
6.31	8.9	4.4—5.1	28	14—16
5.62	10.2	5.7—6.4	32	18—20
4.57	15.2	6.4—7.0	48	20—22
3.39	17.1	7.6—8.3	54	24—26

SOD = Stand-off distance
$R_{noz} = 0.32$ cm (0.125 inches)

7. Results and Discussion

7.1 Flame-Jet Tests

The results of the flame-jet spallation tests are listed in Tables 3 and 4, and illustrated in Figs. 11 and 12 for Barre and Westerly granite, respectively. The curve representing the Weibull theory spallation temperature predictions (Eq. (9)) is obtained by using mechanically-determined Weibull parameters (Dey and Kranz, 1985) and averaged physical properties for Barre and Westerly granite (Table 3). In addition, the theoretical 90% probability interval, defined as the region bounded by the temperature values at which 5% and 95% cumulative probabilities of spalling are predicted to occur, is shown for reference.

At heat fluxes above about 1 MW/m^2 the surface temperatures on Barre granite are higher and more sensitive to heat flux than previously predicted. This suggests that a smaller value of the homogeneity parameter, m, should be used. At 2.9 MW/m^2 the measured surface temperature is about a factor of two higher than the Weibull prediction.

Table 3. Flame-jet spallation surface temperature values — heat flux from energy balance

Barre granite

Stand-off distance (Z_{dr}/R_{noz})	Estimated drilling velocity (V_{dr}) (m/hr)*	Spallation surface temperature ($T_{s,st}$) (K)	Heat flux (Q_{st}) $^+$ (MW/m^2)
32	4.3	925	2.9
40	3.3	937, 937, 837	2.1
47	3.1	879, 850, 930, 890, 785	1.9
63	2.8	710, 700	1.4
80	2.5	520, 520, 508, 520	0.9
96	2.2	475, 520	0.8

Westerly granite

Stand-off distance (Z_{dr}/R_{noz})	Estimated drilling velocity (V_{dr}) (m/hr)*	Spallation surface temperature ($T_{s,st}$) (K)	Heat flux (Q_{st}) $^+$ (MW/m^2)
32	5.6	738	2.9
80	2.9	600	1.2
96	2.5	475, 520	0.9

$R_{noz} = 0.32$ cm (0.125 inches)

$^+$ $Q_{st} = (\rho C_p)_r V_{dr} (T_{s,st} - T_{r0})$,
$(\rho C_p)_r = 2.64 \times 10^6$ J/m^3, and $T_{r0} = 300$ K

* Approximated using experimental data reported by Rauenzahn and Tester (1991b)

Table 4. Flame-jet spallation surface temperature values — heat flux from transient analysis

Barre granite

Stand-off distance (Z_{dr}/R_{noz})	Local spallation surface temperature (T_s) (K)*	Heat flux (Q_w) $^+$ (MW/m^2)
32	785	1.8
47	925	2.0
47	785	1.3
47	808	1.1
47	832	1.4
63	638	0.6
80	588	0.5

$^+$ Heat flux from transient analysis,
$k_r = 2.14$ W/m K, and
$\alpha_r = 0.87 \times 10^{-6}$ m^2/s

* Measured values from point of heat flux measurement

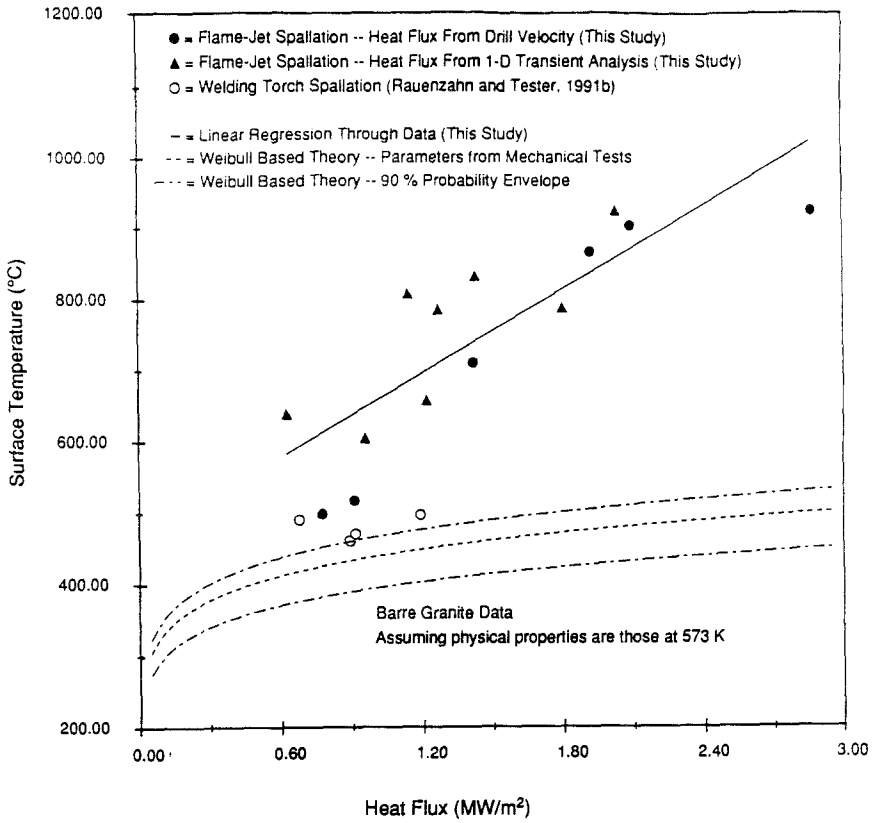

Fig. 11. Spallation surface temperature versus heat flux — flame-jet results in Barre granite. Predictions use averaged Barre and Westerly physical property data: $(\rho C_p)_r = 2.64 \times 10^6$ (J/m³ K), $\beta_r = 9 \times 10^{-6}$ (K^{-1}), $E = 52.5$ (GPa), $\upsilon = 0.25$, $\alpha_r = 0.9 \times 10^{-6}$ (m²/s), $m = 20$, $\sigma_0 = 70$ MPa $-$ m$^{3/20}$

Surface temperatures measured on Barre granite at low heat fluxes (less than about 1 MW/m²) are within experimental scatter of onset temperatures measured in earlier tests (Rauenzahn and Tester, 1991b) using a calibrated welding torch to induce spallation. The consistency of the two sets of results between about 0.6—1.2 MW/m² confirms that the IR scanner is not grossly inaccurate and indicates that at low heat fluxes the spallation onset temperatures may be representative of those achieved during steady spalling. Therefore, one might expect that at a low enough heat flux (and surface temperature rise) the mechanically-obtained Weibull parameters should accurately represent the rock failure that occurs. This behavior is consistent with the welding torch results obtained by Rauenzahn and Tester (1989, 1991b) which agreed with predictions using mechanical Weibull parameters. This point will be further discussed below in the presentation of laser induced spallation results.

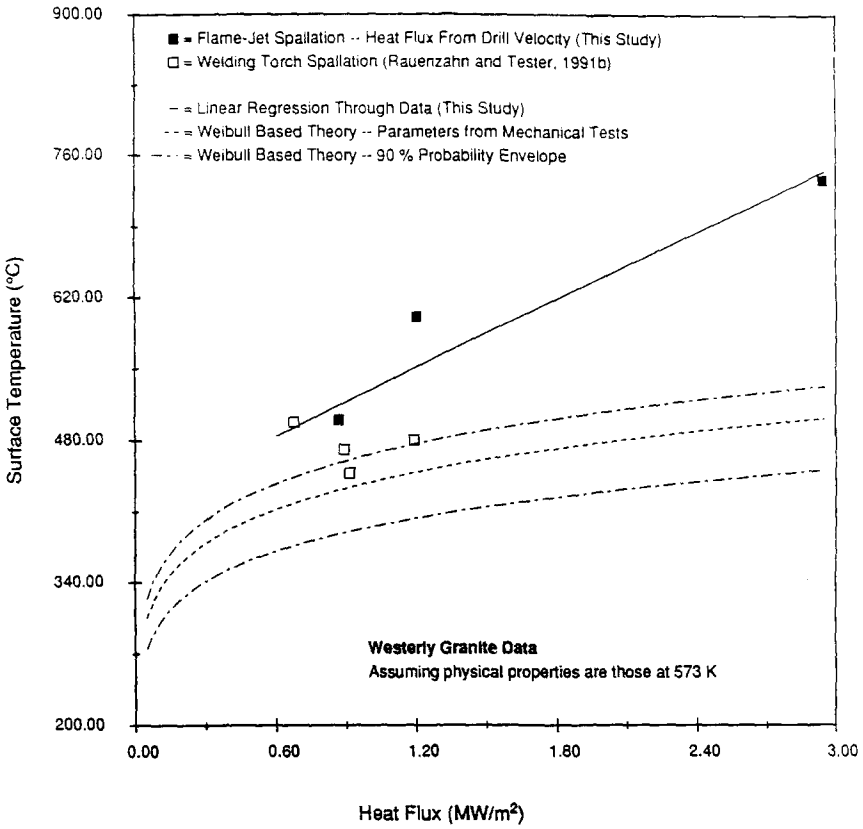

Fig. 12. Spallation surface temperature versus heat flux — flame-jet results in Westerly granite. Weibull based predictions used averaged Barre and Westerly physical property data cited in Fig. 11

Comparison of the results illustrated in Figs. 11 and 12 reveals that spallation temperatures for Barre granite are higher than those for Westerly granite at heat fluxes above approximately 1 MW/m^2. In addition, spallation temperatures for Westerly granite are not as strongly dependent on heat flux as they are for Barre granite, indicating that Westerly granite has a higher homogeneity parameter. This is consistent with the observation that the average grain size in Westerly granite is about one-half of that in Barre granite. For a given thermal penetration depth, more grain boundaries will be encountered in Westerly granite. Therefore, if flaws extend preferentially between grains, more potentially critical flaws will be encountered at a given surface temperature, so a lower spallation temperature should be expected to cause failure. However, the different spallation temperatures at high heat fluxes for Barre and Westerly granite could also potentially be caused by the different mineral compositions and physical properties. Further study is required before firm conclusions can be drawn regarding these differences in spallation temperatures.

Table 5. Measured surface temperatures and calculated heat fluxes from laser spallation experiments

Barre granite

Q (MW/m^2)	T_s(°C)	Q (MW/m^2)	T_s(°C)
0.31	481	0.59	630
0.35	495	1.47	604
0.38	520	1.55	870
0.43	495	1.78	690
0.47	457	1.92	685
0.53	497	1.95	808
0.54	497	2.28	686
0.55	423	2.39	930
0.58	423	2.41	890

Westerly granite

Q (MW/m^2)	T_s(°C)	Q (MW/m^2)	T_s(°C)
0.23	457	1.48	598
0.40	524	1.54	646
0.45	457	1.64	645
0.52	423	1.77	710
0.56	423	1.95	767
1.07	442	2.14	483
1.34	645	2.50	551

Sioux quartzite

Q (MW/m^2)	T_s(°C)	Q (MW/m^2)	T_s(°C)
0.71	361	2.13	364
0.83	364	2.16	364
1.62	331	2.29	350
1.86	350	—	—

$k_r = 3.0$ W/m K
$\alpha_r = 0.9 \times 10^{-6}$ m^2/s (estimated)

Webatuck dolomite

Q (MW/m^2)	T_s(°C)
1.24	504
1.32	457
2.79	598
2.86	551
3.92	645

$k_r = 3.33$ W/m K
$\alpha_r = 0.93 \times 10^{-6}$ m^2/s (from Birch et al., 1942)

7.2 Laser Spallation Tests

Laser spallation tests have been conducted on Barre and Westerly granite, Sioux quartzite, and Webatuck dolomite (Table 5). Measured surface temperatures as a function of heat flux are plotted along with 90% probability envelopes for Barre and Westerly granite in Figs. 13 and 14, respectively.

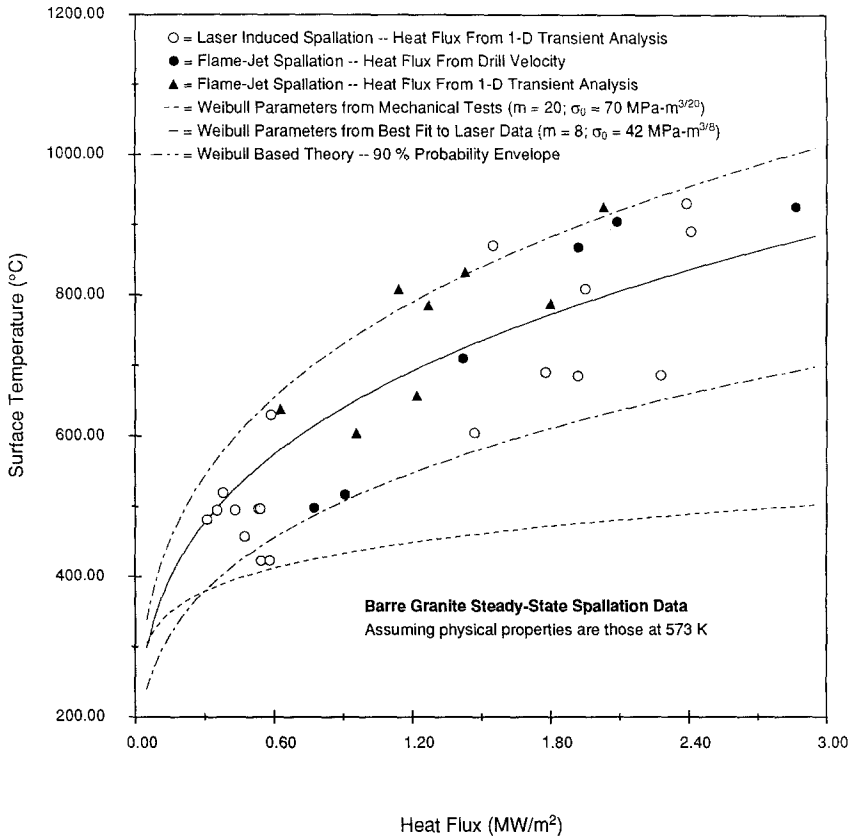

Fig. 13. Surface temperature during steady state spallation versus heat flux for Barre granite — comparison between laser and flame-jet results

Considerable data scatter exists especially for the Westerly granite, but the laser results follow the general trends mapped out by the flame-jet data. The consistency in these trends is a further indication that infrared interference effects did not substantially influence temperature measurements made during flame-jet spallation.

Included in Figs. 13 and 14 are Weibull theory predictions using m and σ_0 parameters fit to the laser data along with the physical properties listed in Table 6. The predicted 90% probability envelopes contain most of the scatter. Specifically, spallation failure at the surface is governed by the stress field and the inherent flaw structure near the surface. The locations for measurements have been chosen arbitrarily in this study so that temperatures should be expected to form a distribution governed by the Weibull statistics rather than conform to a median condition. This is in contrast to the relatively small amount of scatter in the flame-jet stagnation-point temperatures reported in this study where the temperatures are area-weighted averages in the stagnation region of the flow-field.

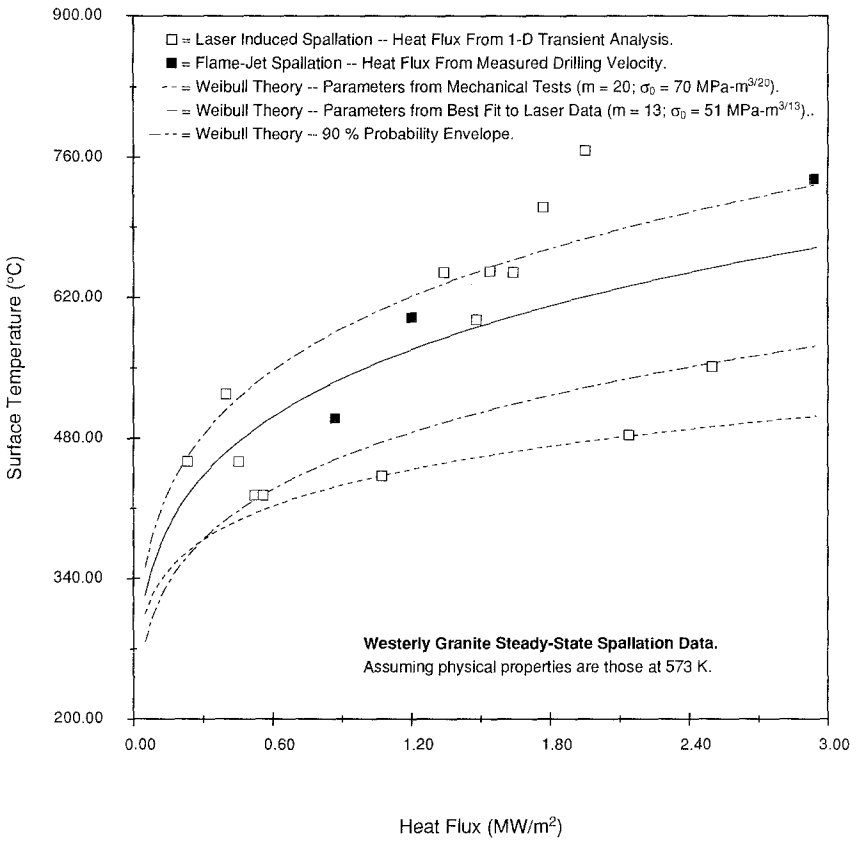

Fig. 14. Surface temperature during steady state spallation versus heat flux for Westerly granite — comparison between laser and flame-jet results

Another factor contributing to the data scatter of the laser results is the relatively coarse time and temperature resolution capabilities of the IR scanner. At a heat flux of 3.0 MW/m^2, spallation times are typically on the order of 150—200 milliseconds and surface temperatures of about 900 °C are achieved. However, the infrared scanner samples at a rate of once every 50 milliseconds and has a temperature resolution capability (for the range required at this heat flux) of about 90 °C. The consequences of this relatively coarse discretization of the temperature history have been investigated by successively removing single data points from some of the transient temperature rise curves and re-calculating the heat fluxes. Variations of up to 35% in the calculated heat flux were found. Therefore, each of the data points presented in Figs. 11—14 with heat flux calculated by the transient analysis (Eqs. (10) and (11)) contains an inherent ±35% uncertainty region with respect to both heat flux and temperature due solely to experimental procedures. This contributes substantially to the observed data scatter.

Sioux quartzite and Webatuck dolomite surface temperature data are also included in Table 5. Sioux quartzite spalls at an average surface temperature of approximately 355 °C and has no measurable dependence on applied heat flux over the range tested (0.7—2.3 MW/m²). Sioux quartzite is approximately 93% pure crystalline quartz and is fine grained (0.2—0.5 mm diameter). Therefore, if the distribution of flaws capable of initiating spallation is related to composition and grain size, the Weibull-based theory described earlier dictates that spallation temperatures should be relatively independent of heat flux. Unfortunately, Weibull parameters obtained from mechanical testing procedures are not available for Sioux quartzite so comparison of experimental surface temperature data with predictions made using Eq. (9) is not possible. In the future, Weibull strength parameters for Sioux quartzite should be experimentally determined.

Table 6. Weibull parameters fit to laser spallation data and 300 K physical property values used for Barre and Westerly granite

Barre granite

Fitted Weibull parameters	Physical properties
$m = 7.7$	$(\rho C_p)_r = 2.64 \times 10^6$ (J/m³ K)
$\sigma_0 = 42$ MPa – m$^{3/7.7}$	$\beta_r = 8.0 \times 10^{-6}$ (K^{-1})
	$E = 47$ (GPa)[a]
	$\nu = 0.27$[a]
	$\alpha_r = 0.9 \times 10^{-6}$ (m²/s)[b]

Westerly granite

Fitted Weibull parameters	Physical properties
$m = 12.8$	$(\rho C_p)_r = 2.64 \times 10^6$ (J/m³ K)
$\sigma_0 = 51$ MPa – m$^{3/12.8}$	$\beta_r = 11 \times 10^{-6}$ (K^{-1})
	$E = 58$ (GPa)[a]
	$\nu = 0.225$[a]
	$\alpha_r = 0.9 \times 10^{-6}$ (m²/s)[b]

[a] From Krech et al. (1974)
[b] from Hanley et al. (1978)

The spallation surface temperatures of Webatuck dolomite vary from 457 °C to 645 °C for heat fluxes ranging from 1.24 MW/m² to 3.92 MW/m². However, it is unclear whether true spallation was occurring during these tests since rock chips were not observed to violently eject from the surface, as they characteristically do during spallation with granite and quartzite. Instead, the rock surface appeared to disintegrate and rock particles dropped off the surface forming a pile a hot material at the base of the sample. The observed behavior indicates that the dolomite, which is approximately 80% $MgCO_3$, may have been reacting to form MgO and CO_2 through a calcination type of mechanism. However, no independent analysis of the residual material has been conducted to confirm this possibility. Since mechanical Weibull parameters are not available for estimation of surface temperatures using Eq. (9), and since the present study was aimed

toward drilling in crystalline rocks, no further investigation of dolomite was performed.

7.3 Global Onset Temperatures

The global onset temperature is defined as the temperature of the rock surface when the first spall is removed from any point on the surface. Values of spallation global onset temperature are seen in Fig. 15 to be relatively insensitive to the applied heat flux level. Furthermore, most of the measured values are within about 30% of those predicted using mechanical Weibull parameters and those reported by Rauenzahn and Tester (1991b). However, above about 1.0 MW/m^2, global spallation onset temperatures are significantly lower than continuous flame-jet temperatures and local laser spallation temperatures. This is again explained by recognizing the stochastic nature of spallation. Since the global onset temperature is that at which the first spall is ejected from *any* point on the surface, it represents the low temperature limit of the statistical distribution. Random, or at least

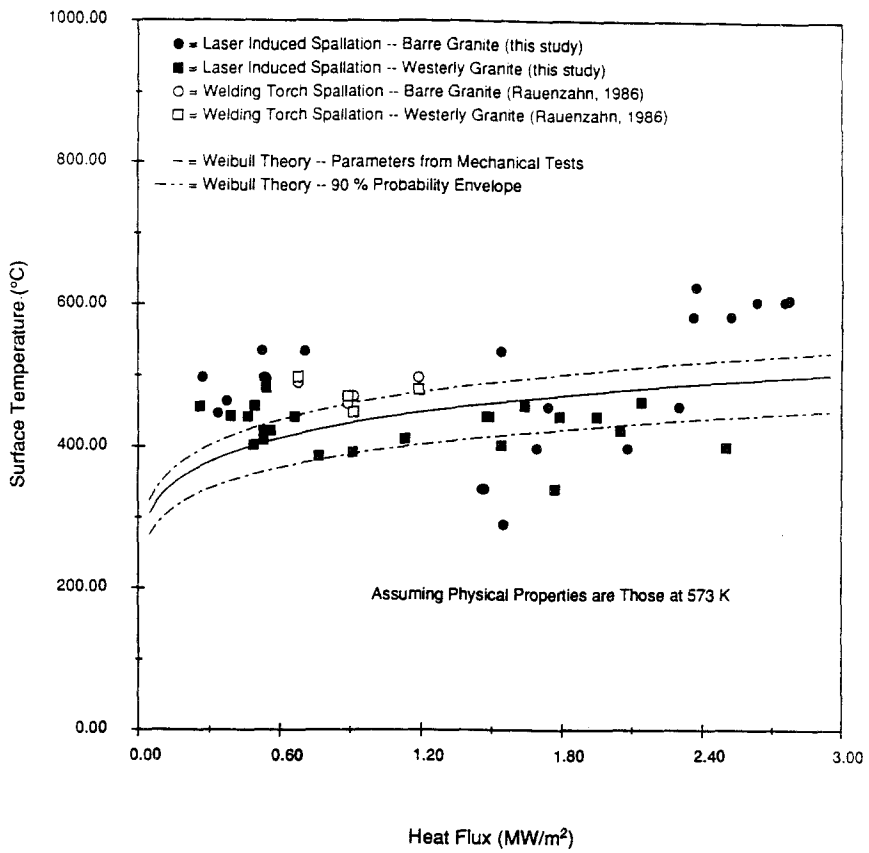

Fig. 15. Global spallation onset temperature versus heat flux

arbitrarily chosen, temperature measurement locations are more useful for determining average surface conditions during spallation drilling.

7.4 Experimentally Determined Stanton Numbers

The value of the surface temperature strongly affects calculated values of experimental Stanton numbers because T_s appears both in the numerator and the denominator of Eq. (5):

$$St_{\text{exp}} = \frac{(\rho\, C_p)_r\, V_{dr}\,(T_s - T_{r0})}{(\rho\, C_p\, U)_{\text{jet}}\,(T_{\text{jet}} - T_s)}. \tag{5}$$

For example, a surface temperature change from 700 K to 100 K with a jet temperature of 2830 K causes more than a two-fold increase in Stanton number if all other variables remain constant.

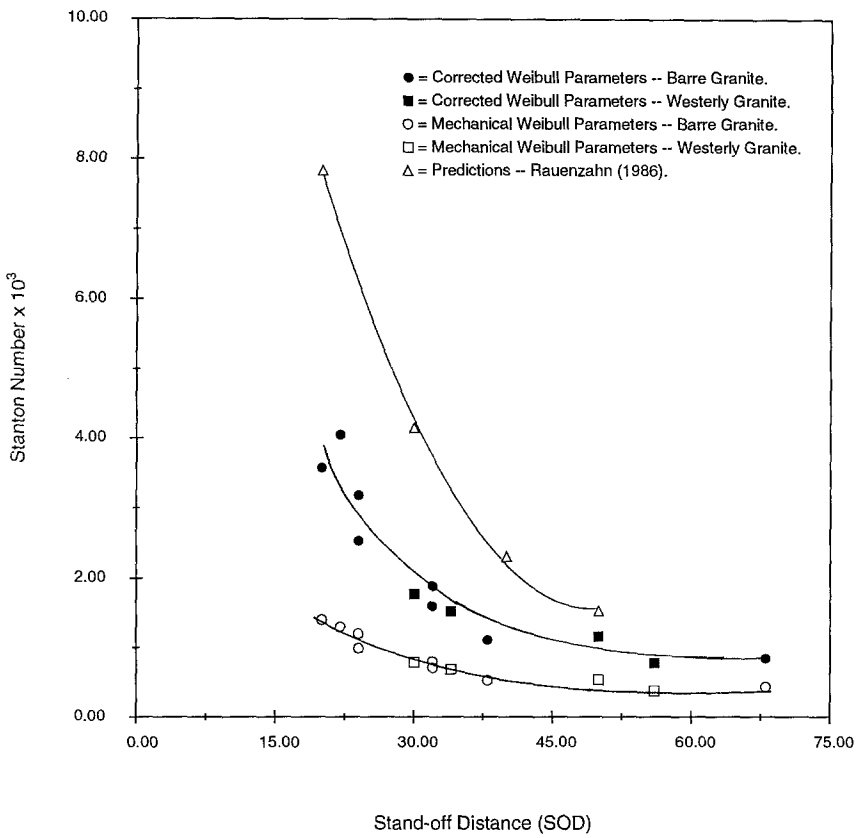

Fig. 16. Comparison of Rauenzahn's (1986) predicted curve of Stanton number versus SOD with curves estimated from field drilling experiments using Weibull parameters obtained in the present study and by mechanical testing procedures

The newly calculated Stanton numbers obtained using values for the penetration rate obtained from earlier field drilling experiments (Rauenzahn and Tester, 1991b) and surface temperatures estimated in the present study are plotted along with old Stanton numbers and prediction of Rauenzahn and Tester (1991b) in Fig. 16. Fitted values of m and σ_0, along with physical property values listed in Table 6 are used for temperature determinations.

The results shown in Fig. 16 for non-dimensional stand-off distance (SOD) values below 26 are of unknown accuracy because the heat fluxes and surface temperatures predicted by Eq. (9) are higher than any that were measurable with the infrared scanner. Surface temperatures calculated for SOD values of 22, 24, and 26 are close to the rock melting temperature (approximately 1050 °C) and may lead to higher calculated Stanton numbers than are actually achieved.

8. Conclusions and Recommendations

The results displayed in Fig. 16 show that experimental Stanton numbers for field drilling experiments are substantially closer to simulation results than those originally reported by Rauenzahn and Tester (1991b). Unfortunately, however, this improvement does not necessarily justify the use of a Weibull-based theory to describe the rock failure mechanism that occurs during thermal spallation. This point is illustrated by considering a possible alternative mechanism to account for the discrepancy between results obtained using mechanical Weibull parameters and those obtained during thermal spallation.

The sequence of events leading to failure by the alternative mechanism shown in Fig. 17 is as follows:

1. crack extension and alignment with the compressive stress field,
2. partial buckling,
3. "overheating" of the spall during the time taken while competition between build-up, due to thermal expansion of the "spall", and stress relief, due to deformations in adjacent "soft" materials, occurs, and
4. spall ejection.

Mechanical Weibull parameters are expected to accurately describe the statistics of steps 1 and 2, but the overheating is a higher-order phenomena that becomes important at high heat fluxes and is not included in mechanical testing procedures normally used to validate the Weibull theory description of rock failure.

The above mechanism is consistent with the few values of spallation temperature obtained in this study for Sioux quartzite (Table 5), where it is observed that onset and steady state spallation temperatures are identical. Sioux quartzite is approximately 93% pure quartz so no appreciable softening or overheating would be expected at the measured surface temperatures. Unfortunately, mechanical Weibull parameters for Sioux quartzite have not been found in the literature for comparison.

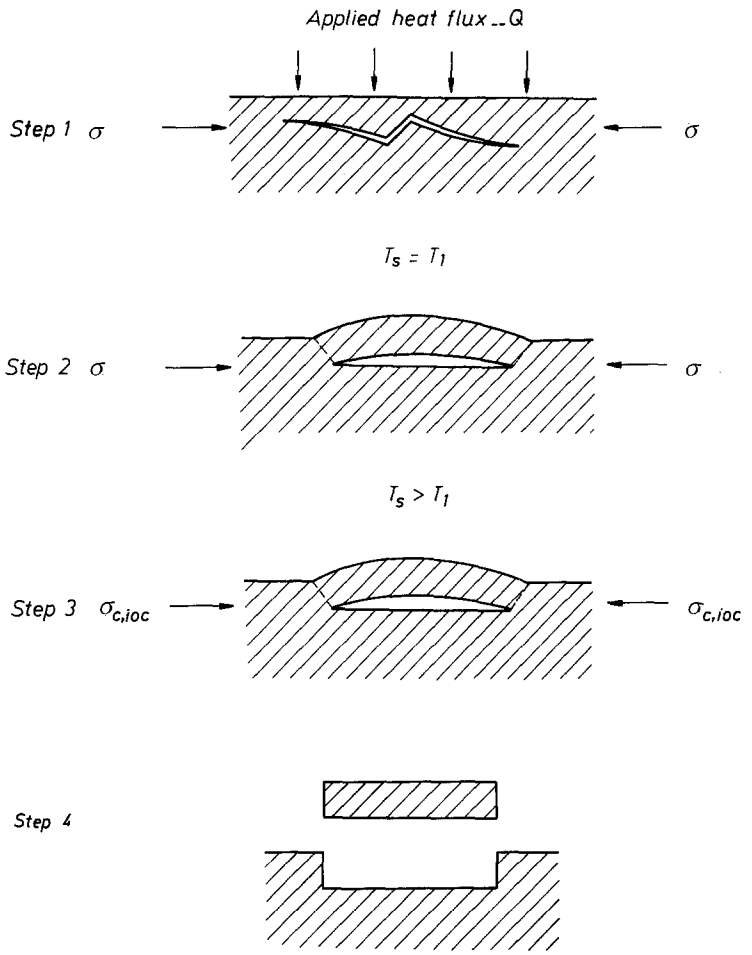

Fig. 17. Illustration of possible mechanism for "overheating" at high heat fluxes

Future work should be directed at increasing the data base for granites and other spallable rocks. Laser heating tests like those performed in this study should be used to investigate the statistical spread of spallation temperatures at a given heat flux. However, high speed IR scanning equipment with a broader temperature measurement range, and higher precision, will be needed to perform meaningful analysis at heat fluxes in excess of about 2 MW/m^2.

Further study of thermal spallation at low heat fluxes will eliminate potential "overheating" effects described above. Tests could be carried out with a subsonic jet, for example a welding torch, or with a large diameter laser. Some researchers theorize that "nonspallable" rocks such as limestone could be spalled if the surface temperatures were kept below the point where ductile, instead of brittle, failure occurs (Potter, 1988). This could be accomplished by using lower heating rates or by pulsing the heat

flux (Williams et al., 1991). Low heat flux spallation using lasers should be used as a method to provide insight into this potential phenomenon. The use of lasers will decrease the coupling that occurs between the heat transfer mechanism and the rock mechanics during flame-jet thermal spallation.

Quantitative correlations for spallation temperature developed in the present study are used in the flow-field simulation model described elsewhere by Wilkinson (1989) and Wilkinson and Tester (1993). For the purposes of flow-field modeling, the surface temperature is assumed to follow Eq. (9) which is based on Weibull theory. The physical properties and Weibull parameters, m and σ_0, used in the simulation model are the averages of Barre and Westerly granite values that were listed in Table 6. These values should provide reasonable surface temperature estimates for the simulation model regardless of whether Weibull theory correctly describes the rock failure mechanism, since the Weibull parameters have been fitted to match experimental data obtained under actual spallation conditions.

Nomenclature

A	slope of best-fit line
C_L	spall diameter: thickness ratio
C_p	constant pressure heat capacity (J/kg K)
E	Young's modulus (MPa); total energy
$G(\sigma)$	cumulative probability of failure
ΔH_{pt}	energy losses due to miscellaneous phase transitions and crack formation (W/m^2)
k_r	rock thermal conductivity (W/m K)
m	Weibull homogeneity parameter
Q_r, Q	local heat flux to rock (W/m^2)
Q_p	predicted heat flux (W/m^2)
Q_{jet}	total jet inlet heat flux (w/m^2)
R_{noz}	nozzle radius (m)
R_h	hole radius (m)
SOD	dimensionless stand-off distance (Z_{dr}/R_{dr})
St	stanton number
St_p	predicted Stanton number based on surface heat flux
St_{exp}	experimental Stanton number based on measured penetration rate
t	time (s)
T	temperature (K)
T_s	local surface temperature (K)
T_{ro}	initial rock temperature (K)
$T_{s,st}$	stagnation point surface temperature (K)
T_{jet}	gas temperature at nozzle outlet (K)
U_{dr}	local drilling velocity normal to rock surface (m/s)

U_{jet} jet velocity (m/s)
V sample volume (m^3)
V_{dr} forward drilling or penetration rate (m/s)
Z_{dr} distance from the bottom of the drill to the stagnation point (m)

Greek letters

α_r thermal diffusivity of the rock (m^2/s)
β_r thermal coefficient of expansion ($V^{-1}(\partial V/\partial T)_\rho$ (K^{-1})
σ local rock stress (MPa)
σ_0 Weibull parameter (MPa – $m^{3/m}$)
ρ_r rock density (kg/m^3)
ν Poisson's ratio

Subscripts

dr drilling related parameters
exp experimental value
jet property at nozzle outlet conditions
noz at nozzle
r rock property
s rock surface property
sp at spallation
st at stagnation point conditions

Acknowledgements

The Authors wish to thank Rick Rauenzahn and Robert Potter of Los Alamos National Laboratory and MIT Professors Judson Baron, Kenneth Smith, and Preetinder Virk for their useful advice and comments. Fred Armellini, Per Cederstav and Charles Grigsby provided much needed and appreciated assistance during the field experiments and Kevin Sparks and Karl Graham were very helpful with software development and other technical issues. Finally, we would like to recognize a number of industrial and government organizations who provided partial financial support and/or technical assistance during this research. These include Air Products and Chemicals Corporation, the Bonner Monument Company, Browning Engineering Corporation, Data General Corporation, Dorchester Marble Company, Los Alamos National Laboratory, the Natural Sciences and Engineering Research Council of Canada, Rock of Ages Corporation, and Sandia National Laboratories.

References

Armstead, H. C. H., Tester, J. W. (1987): Heat Mining, Spon, London.

Birch, F., Schairer, J. F., Spicer, H. C. (ed.) (1942): Handbook of physical constants. Geol. Soc. Amer., Special Paper No. 36.

Browning, J. A. (1981): Flame-jet drilling in Conway, N. H. Granite. Unpublished report Univ. of California, Nr. 4-L10-2889R-1.

Browning, J. A., Horton, W. B., Hartman, H. L. (1965): Recent advances in flame-jet working of minerals. 7th Symp. Rock Mech., Pennsylvania State Univ., University Park.

Calaman, J. J., Rolseth, H. C. (1961): Technical advances expand use of jet-piercing process in Taconite Industry. Int. Symp. Mining Res., Univ. of Missouri, Columbia.

Carslaw, H. S., Jaeger, J. C. (1959): Conduction of heat in solids. Oxford University Press, Oxford.

Dey, T. N. (1984): More on spallation theory. Los Alamos National Laboratory Internal Memorandum No. ESS-3-286-84.

Dey, T. N., Kranz, R. L. (1985): Methods of improving drilling performance of the thermal spallation drilling system. 9th Conf. Geotherm. Energy, Geotherm. Res. Counc. Transactions Vol. 9, Davis, California.

Hanley, E. J., DeWitt, D. P., Roy, R. F. (1978): The thermal diffusivity of eight well-characterized rocks for the temperature range 300 to 1000 K. Eng. Geol. 12, 31—47.

Krech, W. W., Henderson, F. A., Hjelmstad, K. E. (1974): A standard rock suite for rapid excavation research. U. S. Bureau of Mines Report RI-7865.

Potter, R. M. (1988): pers. comm., Los Alamos, New Mexico.

Preston, F. W. (1934): Observations on spalling. J. Am. Ceram. Soc. 17, 137—144.

Rauenzahn, R. M. (1986): Analysis of the rock mechanics and gas dynamics of flame-jet thermal spallation drilling. Ph. D. Thesis, MIT., Cambridge, Massachusetts.

Rauenzahn, R. M., Tester, J. W. (1985): Flame-jet induced thermal spallation as a method of rapid drilling and cavity formation. In: Proc., 60th Assn. Tech. Conf. and Exhibition, Soc. Petrol. Eng. paper 14331, Las Vegas.

Rauenzahn, R. M., Tester, J. W. (1989): Rock failure mechanisms of flame-jet thermal spallation drilling — theory and experimental testing. Int. J. Rock Mech. Min. Sci. Geomech. Abstr. 26 (5), 381—399.

Rauenzahn, R. M., Tester, J. W. (1991a): Numerical simulation and field testing of flame-jet thermal spallation drilling — 1. Model development. Int. J. Heat Mass Transfer 34 (3), 795—808.

Rauenzahn, R. M., Tester, J. W. (1991b): Numerical simulation and field testing of flame-jet thermal spallation drilling — 2. Experimental verification. Int. J. Heat Mass Transfer 34 (3), 809—818.

Tester, J. W., Herzog, H. J. (1990): Economic predictions for heat mining: a review and analysis of hot dry rock (HDR) geothermal energy technology. MIT-EL 90-001, Cambridge, Massachusetts.

Tester, J. W., Herzog, H. J. (1992): The economics of heat mining: an analysis of design options and performance requirements of hot dry rock (HDR) geothermal power systems. Energy Systems Policy 15 (1), 33—63.

Thurumalai, K. (1969): Process of thermal spalling behavior in rocks — an exploratory study. 11th Symp. Rock Mech., Univ. of California.

Weibull, W. (1939): A statistical theory of strength of materials. Invgvetensk. Akad. Handl. 151, 1—45.

Wilkinson, M. A. (1989): Computational modeling of the gas-phase transport phenomena and experimental investigation of surface temperatures during flame-jet thermal spallation drilling. Ph. D. Thesis, MIT, Cambridge, Massachusetts.

Wilkinson, M. A., Tester, J. W. (1993): Computational modeling of fluid flow and heat transfer effects during supersonic flame-jet induced rock spallation (submitted to Int. J. Heat Mass Transfer).

Williams, R. E., Dey, T., Rauenzahn, R. M., Kranz, R., Tester, J. W., Potter, R., Murphy, H. (1988): Advancements in thermal spallation drilling technology. Los Alamos National Laboratory Report LA-11391-MS.

Williams, R. E., Beck, F. E., Potter, R. M. (1991): Thermal spallation drilling research report, Subcontract No. 9-X68-5616R-1. Los Alamos National Laboratory and New Mexico Institute of Mining and Technology.

Author's address: Jefferson W. Tester, Energy Laboratory and Chemical Engineering Department E40-455, Massachusetts Institute of Technology, Cambridge, MA 02139, U.S.A.